Blöcher, G., Cacace, M., Jacquey, A. B., Zang, A., Heidbach, O., Hofmann, H., Kluge, C., Zimmermann, G. (2018): Evaluating Micro-Seismic Events Triggered by Reservoir Operations at the Geothermal Site of Groß Schönebeck (Germany). - *Rock Mechanics and Rock Engineering*, *51*, 10, pp. 3265—3279.

DOI: http://doi.org/10.1007/s00603-018-1521-2

Rock Mechanics and Rock Engineering manuscript No.
(will be inserted by the editor)

Evaluating micro-seismic events triggered by reservoir operations at the geothermal site of Groß Schönebeck (Germany)

Guido Blöcher · Mauro Cacace · Antoine B. Jacquey · Arno Zang · Oliver Heidbach · Hannes Hofmann · Christian Kluge · Günter Zimmermann

Received: date / Accepted: date

Abstract This study aims at evaluating the spatial and temporal distribution of 26 micro-seismic events which were triggered by hydraulic stimulation at the geothermal site of Groß Schönebeck (Germany). For this purpose, the alteration of the in-situ stress state and the related change of slip tendency for existing fault zones due to stimulation treatments and reservoir operations is numerical simulated. Changes in slip tendency can potentially lead to reactivation of fault zones, the related movement can lead to the occurrence of seismic events. In the current numerical study, results obtained based on the thermal-hydraulic-mechanical coupled simulation are compared to field observations. In particular, the study focuses on describing the fault reactivation potential: (i) under in-situ stress conditions, (ii) during a waterfrac stimulation treatment, and, (iii) during a projected 30 years production and injection period at the in-situ geothermal test-site Groß Schönebeck. The in-situ stress state indicates no potential for fault reactivation. During the waterfrac stimulation treatment micro-seismic events were recorded. Our current evaluation shows an increase of slip tendency during the treatment above the failure level in the direct vicinity of the micro-seismic events. During the projected production and injection period, despite increased thermal stress, the values for slip tendency are below the threshold for fault reactivation. Based on these results, and in order to prove the applied method to evaluate the observed micro-seismic events a final discussion is opened. This includes the in-situ stress state, the role of pre-existing fault zones, the adopted criterion for fault reactivation, and a 3D rock failure criterion based on true triaxial measurements.

Keywords fault reactivation · enhanced geothermal systems · induced seismicity · Thermal-Hydraulic-Mechanical (THM) simulation

Corresponding author. E-mail address: Guido.Bloecher@gfz-potsdam.de (G. Blöcher).

Guido Blöcher · Mauro Cacace · Antoine B. Jacquey · Arno Zang · Oliver Heidbach · Hannes Hofmann · Christian Kluge · Günter Zimmermann
Helmholtz Centre Potsdam - GFZ German Research Centre for Geosciences

Abbreviations
BHP Bottom Hole Pressure
CCS Carbon Capture and Storage
EGS Enhanced Geothermal System
EU European Union
$GEISER$ Geothermal Engineering Integrating Mitigation of Induced Seismicity in Reservoirs
KTB Kontinentales Tiefbohrprogramm der Bundesrepublik Deutschland
ST Slip Tendency
$TCDP$ Taiwan Chelungpu-fault Drilling Project
THM Thermal-Hydraulic-Mechanical
$TVDSS$ True Vertical Depth SubSea
UTM Universal Transverse Mercator coordinate system

List of Roman Symbols
A material constant
B material constant
c_f fluid heat capacity
K_f fluid modulus
K_s solid modulus
M_b Biot modulus
n_1, n_2, n_3 components of the normal unit vector
p_f reservoir fluid pressure
S_0 cohesion
S_{Hmax} maximum horizontal stress
S_{hmin} minimum horizontal stress
S_V vertical stress
T temperature
t time
$\boldsymbol{g}$ gravitational acceleration vector
$\boldsymbol{k}$ permeability tensor
$\boldsymbol{q_D}$ Darcy velocity vector
$\boldsymbol{u}$ displacement vector

List of Greek Symbols
α Biot's poroelastic coefficient
β_b bulk volumetric thermal expansion coefficient
$\boldsymbol{\epsilon}$ strain tensor
$\boldsymbol{\sigma'}$ effective stress tensor
λ_b bulk thermal conductivity
μ_f fluid viscosity
μ_s coefficient of friction
ϕ porosity
ρ_b bulk density
ρ_f fluid density
σ'_m mean effective stress acting on the plane of failure

$\sigma_1, \sigma_2, \sigma_3$ principle stresses
σ_n normal stress
σ'_n effective normal stress
τ shear stress
τ'_{oct} octahedral shear stress
$(\rho c)_b$ bulk specific heat

List of other Symbols
∇ nabla operator
$\mathbb{C}$ rank-four elastic stiffness tensor
$\mathbb{1}$ rank-two identity tensor

1 Introduction

1.1 Induced seismicity

Induced seismicity is a phenomenon critical to the success of any Enhanced Geothermal System (EGS) development. Mapping induced seismicity hypocentres with high precision (tens of meters) allows to image and estimate the geometry and dimensions of the fracture network generated at depth during hydraulic stimulation of geothermal reservoirs (Fehler et al, 2001). On the other hand, induced seismicity is identified as a potential hazard, with a number of international projects lately being suspended due to public concern, e.g. in Basel (Giardini, 2009; Häring et al, 2008) or in St Gallen (Obermann et al, 2015), Switzerland.

Induced seismicity can arise from a number of man-made activities (Trifu, 2010) including: (i) reservoir-induced by loading of the reservoir and/or by the effect of reservoir fluid pressure (Talwani and Acree, 1985), (ii) mining-induced (Mendecki, 2012), and, (iii) seismicity related to fluid injection and withdrawal of fluid or gas from the Earth's crust. The latter source of induced seismicity can be subdivided into oil and gas operations (Suckale, 2009), waste-water disposal (Ellsworth, 2013), Carbon Capture and Storage (CCS) (Zoback and Gorelick, 2012), and geothermal energy development (Zang et al, 2014).

In the framework of the EU project GEISER, Zang et al (2014) analyzed induced seismicity related to geothermal operations in different tectonic settings. The seismic response to fluid injection was evaluated for different European and worldwide EGS sites, and compared to wastewater disposal, hydraulic fracturing and ultra-deep fluid injection (continental deep drilling project, KTB) data. This comparative study demonstrated that, compared to waste water disposal wells, EGS stimulation involves less fluid volume thus resulting in smaller maximum magnitudes. In reservoirs with multiple stimulation wells, no seismicity is usually triggered until the stress level of previous stimulation is exceeded following the well known Kaiser Effect (e.g. Lavrov, 2003).

During EGS stimulation, larger magnitude events often occur after shut-in at greater distances from the injection well (Baisch et al, 2010; Deichmann et al, 2014). Independent of geologic differences, the probability of such events increases with volume of injected fluids. A differentiation between long-term injection operations (reservoir impoundment (Gupta, 2011), wastewater disposal (Healy et al, 1968)) generating relatively larger events and short-term fluid injection operations

is needed. Regarding the short-term injections, EGS stimulations have in general shown a higher propensity to produce larger events, compared to hydraulic fracturing in oil and gas operations.

EGS development in weak volcanic or sedimentary rocks (e.g., Berlin, El Salvador (Kwiatek et al, 2014), Groß Schönebeck (Kwiatek et al, 2010)) may be different from the permeability enhancement process in crystalline rocks (e.g., Basel (Häring et al, 2008; Deichmann and Giardini, 2009), Cooper Basin (Baisch et al, 2006, 2009), Soutz-sous-Forets (Dorbath et al, 2009; Calò et al, 2014)). While in hard rock dilatant shear may be the dominating failure mechanism in EGS stimulation, in sedimentary formations sub-critically stressed tensile cracks may be generated instead. A careful analysis of the individual fracture mechanism in different geothermal reservoirs is therefore required (Jung, 2013).

1.2 In-situ stress state

The in-situ stress state is the undisturbed natural stress state of the reservoir (Engelder, 1993; Zang and Stephansson, 2010). In order to explore and safely develop a geothermal reservoir it is important to assess its mechanical stability e.g. how far the system is to the stress state required to reactivate pre-existing faults (Morris et al, 1996) and/or to generate new fractures. Furthermore, the in-situ stress state is also important to plan stable borehole pathways and to predict the propagation direction of new fractures during stimulation in order to enhance permeability (Bell, 1996; Fuchs and Müller, 2001; Zoback, 2010). Man-made stress changes due to drilling, production and injection of fluid can also be used to assess the change of occurrence rate of induced seismic events (Hakimhashemi et al, 2014a,b). Details and an overview of statistical and deterministic approaches that can be used to forecast induced seismicity is given in Gaucher et al (2015).

1.3 Fault reactivation potential

As previously discussed, geothermal operations can potentially lead to induced seismicity. Furthermore, by altering the in-situ stress state in the reservoir due to fluid pressure and temperature changes, such changes can finally lead to reactivation of pre-existing fault zones. Reactivation of faults and fracture planes and associated seismicity during geothermal operations strongly depends on the initial stress conditions acting on such plane of weakness. Typically, a slip tendency analysis (ST analysis henceforth) is performed to assess the reactivation potential of these structures or of any other plane of weakness, such as bedding, and to identify those planes which are most prone to reactivation under ambient stress forcing conditions. ST analysis is based on the notion that reactivation and slip on a fault or fracture is controlled by the ratio of the resolved shear stress and effective normal stress on the fault or fracture surface. ST is, therefore defined as the ratio between the absolute shear and normal effective stress magnitudes acting on the fault plane (see e.g. Morris et al (1996)) as:

$$ST = \frac{\|\tau\|}{\|\sigma_n - \alpha p_f\|} = \frac{\|\tau\|}{\|\sigma'_n\|} \tag{1}$$

where τ is the shear stress magnitude, σ_n is the normal stress acting on the plane of weakness, p_f is the reservoir fluid pressure, and α is the effective stress coefficient, also called Biot's poroelastic coefficient. Its upper threshold value is $\alpha = 1$ resulting in Terzaghi's effective stress law, $\sigma'_n = \sigma_n - p_f$. Often α is taken as a constant, but it may be itself a function of the stress state, reservoir fluid pressure and microstructural changes (Blöcher et al, 2009). The quantity appearing as denominator in the above equation represents the effective normal stress σ'_n acting on the fault plane.

Based on equation 1, slip will occur when the shear stress inducing slip along the fault planes exceeds the shear strength of the fault, which can be described based on the Mohr-Coulomb failure criterion as (Labuz and Zang, 2012):

$$\tau \geq S_0 + \mu_s \cdot \sigma'_n \tag{2}$$

$$ST \geq \frac{S_0}{\sigma'_n} + \mu_s \tag{3}$$

where S_0 is the cohesion of the fault and μ_s is the coefficient of friction of the fault.

For a cohesionless fault ($S_0 = 0$) slip will occur when:

$$ST \geq \mu_s \tag{4}$$

Byerlee (1978) experimentally determined μ_s to be greater than or equal to 0.85 for confining pressure up to 200 MPa and $\mu_s \geq 0.6$ at higher confining pressure conditions. Faults containing minerals such as phyllosilicates may have friction coefficients lower than 0.6 (Zoback, 2007). Once the slip tendency is known, it is possible to compute how much fluid pressure increase the fault can withstand before failure occurs.

The slip tendency of a fault or a fracture depends on their orientation with respect to the in-situ stress field. Considering the principal stress axes as the coordinate system, the orientation of the fault plane can be defined by the three directional cosines of the unit vector normal to the fault plane, i.e. n_1, n_2 and n_3.

The shear and effective normal stresses on the fault plane can then be computed from (Jaeger et al, 2007):

$$\sigma'_n = n_1^2\sigma'_1 + n_2^2\sigma'_2 + n_3^2\sigma'_3 \tag{5}$$

$$\tau = \sqrt{n_1^2 n_2^2(\sigma_1 - \sigma_2)^2 + n_2^2 n_3^2(\sigma_2 - \sigma_3)^2 + n_3^2 n_1^2(\sigma_3 - \sigma_1)^2} \tag{6}$$

2 The in-situ geothermal test-site Groß Schönebeck

This study presents the evaluation of slip tendency based on a multistage modelling of the 3D in-situ stress state and its spatial and temporal alteration due to hydraulic stimulation and reservoir operations for the in-situ geothermal test-site Groß Schönebeck (Blöcher et al, 2016). The model area of the reservoir model is 4 $\times$ 4 km^2 and includes sufficient data to characterize the present-day in-situ stress state of the reservoir both in terms of the orientation of S_{Hmax}, the maximum horizontal stress, as well as data records with information on the magnitude of S_{hmin},

the minimum horizontal stress, as derived from leak-off tests. The stress regime at the geothermal test-site Groß Schönebeck is interpreted to be transitional from normal ($S_V > S_{Hmax} > S_{hmin}$) to strike-slip ($S_{Hmax} > S_V > S_{hmin}$) faulting, with values of S_{Hmax} in the sandstones slightly lower than S_V and S_{Hmax} values in the volcanic rocks slightly higher than S_V (Moeck et al, 2009). Given the fact that lateral variations in rock density, and therefore strength, are small in the reservoir section, we consider the vertical stress (S_V) as a principal stress together with both the minimum and maximum horizontal stresses.The in-situ stress state estimated from field measurements at the site is summarized in Table 1. In the sandstone section (4035 m TVDSS), leak-off tests reported a minimum horizontal stress of approximately S_{hmin}=55 MPa. Similar tests in the volcanic rock section of the reservoir, approximately 100 m below, led to a S_{hmin} magnitude of around 72 MPa. This leads to a stress gradient of 0.17 MPa/m that hinders a calibration of both measurements by a unique model, if relying on proper ranges of variation of rock and fluid properties. Therefore, in the following we present two scenarios, that is, (**scenario one**) as calibrated with respect to the data derived for the sandstone section; and, (**scenario two**) calibrated on the data derived for the volcanic rock section.

INSERT TABLE 1 HERE

3 Methods

In order to evaluate the thermal, hydraulic and mechanical response due to a waterfrac stimulation treatment (Zimmermann et al, 2010) and due to a projected 30 years production and injection period at the geothermal research well GtGrSk4/05 in Groß Schönebeck, a numerical investigation of the reservoir has been carried out. Such investigation relies on modeling implicitly coupled and non-linear Thermal-Hydraulic-and Mechanical processes (THM processes hereafter) within a fractured porous reservoir. In this study we rely on the GOLEM simulator (Cacace and Jacquey, 2017) that builds on the flexible, object oriented MOOSE framework (Gaston et al, 2009). Using this approach, fractures are considered as being of lower dimension (2D structures) than the hosting deformable 3D porous rock and their hydraulic aperture is then used as scaling parameter to ensure continuous exchange of fluid mass and energy within the fracture-solid matrix system (Cacace and Jacquey, 2017). In what follows, the governing equations of groundwater flow, heat transport and rock deformation are briefly described, more information on their numerical implementation is provided in Cacace and Jacquey (2017).

The governing equation for reservoir fluid pressure p_f results from the fluid mass balance:

$$\frac{1}{M_b}\frac{\partial p_f}{\partial t} + \nabla \cdot \boldsymbol{q}_D = 0 \tag{7}$$

where $\frac{1}{M_b} = \frac{\phi}{K_f} + \frac{(\alpha-\phi)}{K_s}$ is the specific storage of the porous medium (reciprocal of the Biot modulus M_b) and $\boldsymbol{q}_D = -\frac{\boldsymbol{k}}{\mu_f} \cdot (\nabla p_f - \rho_f \boldsymbol{g})$ is the Darcy velocity. In equation 7, K_f, K_s, α, ϕ, $\boldsymbol{k}$, μ_f, ρ_f, and $\boldsymbol{g}$ denote fluid and solid moduli,

Biot coefficient, porosity, permeability tensor, fluid viscosity, fluid density and gravitational acceleration.

The governing equation for temperature T results from the energy balance of the porous-fracture system under thermal equilibrium conditions as:

$$(\rho c)_b \frac{\partial T}{\partial t} + \nabla \cdot (\rho_f c_f \boldsymbol{q}_D T - \lambda_b \nabla T) = 0 \tag{8}$$

where $(\rho c)_b$ is the bulk specific heat and c_f and λ_b denote fluid heat capacity and bulk thermal conductivity.

The governing equations for the displacement vector $\boldsymbol{u}$ result from momentum balance in terms of effective stress $\boldsymbol{\sigma}'$:

$$\nabla \cdot \left(\boldsymbol{\sigma}' - \alpha p_f \mathbb{1}\right) + \rho_b \boldsymbol{g} = 0 \tag{9}$$

where $\mathbb{1}$ is the rank-two identity tensor, ρ_b is the bulk density of the fluid-solid mixture ($\rho_b = \phi\rho_f + (1-\phi)\,\rho_s$). Following Biot's theory, (effective) stresses are related to mechanical and thermal strain resulting in the following relation:

$$\dot{\boldsymbol{\sigma}}' = \mathbb{C} : \left(\dot{\boldsymbol{\epsilon}} - \frac{\beta_b}{3}\dot{T}\mathbb{1}\right) \tag{10}$$

where $\mathbb{C}$ is the rank-four elastic stiffness tensor, and β_b the bulk volumetric thermal expansion coefficient. To simplify the presentation of the constitutive mechanical model, only small strain conditions are considered resulting in the following strain-displacement ($\boldsymbol{\epsilon} - \boldsymbol{u}$) relation:

$$\boldsymbol{\epsilon} = \frac{1}{2}\left(\nabla \boldsymbol{u} + \nabla^T \boldsymbol{u}\right). \tag{11}$$

This approach was applied to quantify the impact of thermal, hydraulic and mechanical processes at the in-situ geothermal test-site Groß Schönebeck. In order to represent the structural and material information of the site the model as presented by Blöcher et al (2010) was used and extended by considering the mechanical response to geothermal operations (Jacquey et al, 2016).

4 Results

4.1 Fault reactivation potential under in-situ stress conditions

In order to consider the spatial variations of the stress field as well as the accurate geology of the reservoir, a 3D thermal-hydraulic-mechanical simulation of the natural reservoir state was carried out. By means of such a simulation, relative changes of the stress field in the vicinity of faults can be taken into account as well as relative changes in slip tendency along their surfaces. The in-situ stress state (Moeck et al, 2009) (see Table 1) were used to calibrate the simulations. For this purpose the estimated vertical stress S_V was imposed by applying a constant load at the top of the reservoir. Kinematic boundary conditions in terms of displacement were applied at the model boundaries to reach the transitional regime from normal to strike-slip faulting. Values of imposed displacement were changed until the in-situ stress state in the reservoir matched the field observations (Table 2).

INSERT TABLE 2 HERE

Scenario one, calibrated against the stress state in the sandstone section was determined with an absolute error of less than 0.2% for all the three principal stresses (Table 2). This translates into a difference between modeled and measured values of approximately 13 MPa in S_{hmin} in the volcanic rock section. In more detail, the modeled value of S_{hmin} is lower than given in the Moeck et al (2009). For **scenario two**, calibrated for the volcanic rock section, the absolute error amount to less than 0.5% leading to a similar difference in S_{hmin} magnitudes as obtained for the results calibrated for the sandstone section.

Figures 1 and 2 show the results of the slip tendency analysis under in-situ stress conditions as calibrated for the sandstone section (**scenario one**) and the volcanic rock section (**scenario two**). ST values illustrated as a stereo plot (Figure 1a and Figure 2a) for the different faults were obtained by projection of the in-situ stress onto their best fitting plane. For the pre-existing major faults striking NW-SE the slip tendency is relatively far from failure. In contrast minor fault striking NE-SW show higher reactivation potential and are critically stressed for **scenario one** at the top of the reservoir.

INSERT FIGURE 1 HERE

INSERT FIGURE 2 HERE

The stereo plot (Figure 1a) illustrates the slip tendency of the faults in the Lower Permian Rotliegend sandstone beds at 4035 m TVDSS for **scenario one**. Slip tendency values obtained for **scenario two** in the underlying volcanic rocks (Figure 2a) show a similar trend, being characterized by lower absolute magnitudes. Based on the in-situ stress state (see Section 2), faults dipping steeply (45° to 75°) in the direction of S_{hmin} and vertical NE-SW or NNW-SSE striking faults can be considered to be critically oriented for normal and strike-slip faulting, respectively (as indicated by the red areas in the stereo plots). The slip tendency for such faults is estimated to be close to failure, though for both scenarios, none of the faults reached the critical value of 0.85. This suggests that these fault orientations are less than critically stressed under the in-situ stress state and only additional reservoir fluid pressure and/or (e.g. tectonic) stress perturbations may cause these faults to slip.

Figure 1b and Figure 2b show slip tendency variations along the fault surfaces as obtained by models calibrated with respect to the stress state of **scenario one** and **scenario two**, respectively. The calculated slip tendency indicates a higher fault reactivation potential for **scenario one** compared with **scenario two**.

In contrast to the fault reactivation potential under in-situ stress conditions, stimulation treatment or reservoir operation can change the slip tendency in time. Thus, slip tendency (values and their temporal and spatial variations) can be used as an indication for the likelihood of fault reactivation and associated induced seismicity.

4.2 Alteration of in-situ stress state during stimulation

A waterfrac stimulation treatment was carried out in the low permeable volcanic rock section of the geothermal research well GtGrSk4/05 in Groß Schönebeck in 2007 (Zimmermann et al, 2010). A cyclic flow rate was applied with flow rates up to 9 m^3/min. During the high flow rates a friction reducing agent was used in the well to limit the maximum well head pressure to 58.6 MPa (see Figure 3a). To avoid iron scaling of the injected water, acetic acid was added to reduce the pH to 5. During the high flow rates low concentrations of quartz sand (20/40 mesh size) were added to support a sustainable fracture width. Transport of the sand in the fracture and the well was realized solely due to the high flow velocity. The addition of a gel to support the transport was not an option due to the pH restriction.

In total, 13,170 m^3 of fluids and 24.4 tons of meshed quartz sand were injected into the volcanic rocks. A maximum well head pressure of 58.6 MPa was achieved at the maximum flow rate of 9 m^3/min (150 l/s). The total duration of the treatment was 5 days (Zimmermann et al, 2010). Based on the applied flow rate and the corresponding well head pressure the average width of the induced fracture was simulated using the 3D fracture simulator FRACPRO (Zimmermann et al, 2010). Fracture permeability in the range from 2E-06 m^2 to 8E-04^2 was calculated applying the cubic law by means of the average fracture width (0.4 to 2 cm) and assuming only laminar flow conditions. Both quantities, the average fracture width and the corresponding fracture permeability (Figure 3c) were then used as varying material properties for a THM simulation of the waterfrac stimulation treatment.

The validation of the simulation results were based on a comparison to the Bottom Hole Pressure (BHP) during the treatment. Unfortunately, no pressure recording at the bottom hole was performed in the field due to safety reasons. Instead, the operator provided BHP values based on the well head pressure and calculated frictional losses in the well. Furthermore, the 3D fracture simulator FRACPRO provides BHP values using a similar approach considering frictional losses due to laminar and turbulent flow. Both calculated BHP curves show a similar trend with some differences in peak magnitudes (Figure 3d). These differences could mainly be related to the usage of a friction reducing agent during the waterfrac stimulation treatment, which was not considered during the FRACPRO simulations. The simulation results regarding the BHP were obtained by imposing the calculated average fracture width and permeability evolution as input material parameters. Furthermore, the permeability of the volcanic rocks was set four times higher than presented in previous simulations (Blöcher et al, 2010). This was done in an attempt to consider the dependence of the permeability of the volcanic rocks on the effective stress. Due to the reservoir fluid pressure increase, the effective stress will be reduced thus leading to an increase in permeability. For the values adopted in this study, an adequate fit between calculated and simulated values could be obtained (Figure 3d).

INSERT FIGURE 3 HERE

During the hydraulic stimulation micro-seismicity was recorded mainly occurring during the 4th and 5th pressure cycle (Figure 3b). These micro-seismic events with moment magnitudes ranging from -1.0 to -1.8 were recorded with a seismic

network consisting of seven three-component seismometers, including a downhole 3C seismometer operated at 3800 m depth in the neighboring borehole GrSk3/90, 500 m from the injection point (Moeck et al, 2009; Kwiatek et al, 2010). During the 4th pressure cycle 20 micro-seismic events were recorded. These events firstly occurred in the volcanic rock section and then propagated upwards into the sandstone section. During the 5th pressure cycle the 6 recorded events predominantly occurred in the volcanic rock section without any indication of directional propagation.

The analysis of micro-seismic data and 2D seismic profiles indicates that slip during hydraulic stimulation probably occurred on a pre-existing fracture plane with a NNE 014° strike and 52° SE dip (Moeck et al, 2009). A re-calculation of the pre-existing fracture plane performed for this study results in a NNE 018° strike and 55° SE dip. The orientation of this fault plane is consistent with the results of the slip tendency analysis (see Figure 1a), which identified NNE-SSW striking faults with dips between 50°-60° as prone to reactivation under a normal faulting mode. Based on the in-situ stress state in the volcanic rock section (see Table 1) and the geometry of the plane of weakness a slip tendency of 0.68 and 0.38 can be calculated for **scenario one** and **scenario two**, respectively. Based on these results, an increase in reservoir fluid pressure of approximately 6.2 MPa (**scenario one**) and approximately 21.4 MPa (**scenario two**) would lead to a reactivation of the fault. During the waterfrac stimulation treatment a maximum in overpressure between 48 MPa (FRACPRO calculation) and 53 MPa (operator calculation) were generated leading to micro-seismic events. This overpressure was calculated for the wellbore. In contrast, maximum of simulated reservoir fluid pressure increase in the vicinity of the seismic events could be observed at the bottom tip of their best fitting plane (Figures 4a-b). For this point a detailed analysis of the reservoir fluid pressure, temperature, and slip tendency due to waterfrac stimulation treatment was carried out (Table 3). At this point a maximum reservoir fluid pressure increase of ($\Delta p_f = 8.1$ MPa) can be observed. During the waterfrac stimulation treatment, no changes in temperature in the vicinity of the micro-seismic events were modeled. Therefore, thermal stresses can be considered as not impacting the stability of the failure plane, that is, changes in slip tendency can be considered as resulting from reservoir fluid pressure changes only. Induced reservoir fluid pressure changes are similar for both scenarios. At the end of the 4th pressure cycle a slip tendency of 0.92 and 0.42 were calculated for **scenario one** and **scenario two**, respectively (Figures 4c-f). The increase of reservoir fluid pressure for **scenario one** would lead to fault reactivation, which possibly explains the recorded micro-seismic events. In contrast, the slip tendency analysis for **scenario two** does not indicate potential for fault reactivation. It is worth mentioning, that both scenarios assume a pre-existing fault plane geometrically represented by the best fitting plane of the micro-seismic events. However, such fault was not consider to have any specific hydromechanic role in the modeling stage. This choice is consistent with the current geological interpretation of the fault patters in the reservoir (Moeck et al, 2009), see also our final discussion in this regard. However, it is likely that the presence of such a discontinuity would have led to an increase in reservoir fluid pressure diffusion (both in magnitudes and rate of pressure build up) along the fault plane, which would have resulted in a preferential upward propagation of overcritical slip tendency in agreement with the spatial and temporal pattern of the recorded micro-seismicity.

INSERT FIGURE 4 HERE

INSERT TABLE 3 HERE

4.3 Alteration of in-situ stress state during production and injection

During fluid injection and production in a geothermal doublet system the reservoir fluid pressure and temperature change. Injection leads to an increase of reservoir fluid pressure resulting in a decrease of effective normal stress. In contrast, production leads to a decrease in reservoir fluid pressure resulting in an increase of effective normal stress. Such reservoir fluid pressure dynamics likely affect the stability of existing discontinuities, especially in the direct vicinity of the two operating wells. In addition, injection of colder than reservoir conditions water will also lead to the build up of thermal stresses that will impact the effective stress in the reservoir. In particular, the injecting cold water will lead to a decrease of effective normals stresses on the faults. Although it is nowadays established that the ratio between thermo-elastic and poro-elastic stresses increases with increasing rock stiffness and therefore depth, the additional thermal stresses during geothermal operations are usually neglected when analyzing slip potential of pre-existing faults. Numerical studies on the evolution of thermal stress due to cold water injection showed how the induced cooling will lead to a stress reduction, a stress redistribution, and possibly stress rotation (Jeanne et al, 2015). More recent studies have also demonstrated that such changes in the effective stress might extend over a larger areas than under isothermal conditions. Furthermore, reservoir fluid pressure and temperature changes as well as fault dip angle were evaluated by Jacquey et al (2015) to quantify changes in slip tendency. In the particular case of the Groß Schönebeck reservoir Jacquey et al (2016) indicated that the additional thermal stresses exceed the poro-elastic stresses by a factor of ten. To quantify these effects, transient simulations based on the results obtained by **scenario one** were performed. **Scenario one** is considered as the most representative stress state in the reservoir as based on the results discussed in the previous paragraphs.

The aim of simulating 30 years of production and injection is to represent a prospected heat extraction at the geothermal research site Groß Schönebeck and its impact on fault reactivation. In the operational scenario water was produced with a constant rate of 30 m^3/h and injected into the deep portion of the well at 70 °C with a constant rate of 30 m^3/h. All thermal, hydraulic, mechanical, and fluid parameters were based on literature values (Moeck et al, 2009; Blöcher et al, 2010, 2015). Since reservoir fluid pressure and temperature changes tend to be mostly localized in the vicinity of the operating wells, Figure 5a illustrates the changes in slip tendencies for a domain of finite extension between the two wells after 30 years of production and injection.

INSERT FIGURE 5 HERE

A reduction of approximately 20°C (the initial reservoir temperature was around 150°C) causes an increase in slip tendency along the fault within a domain delimited by the cold water front areal extension. Figure 5b shows the distribution of the induced thermal stress due to the injection of cold water which leads to a reduction of effective normal stress on the fault planes. The domain of increased thermal stresses coincides with the geometry of the thermal front moving from the injection towards the production well, thus explaining the differences observed in the slip tendency at those locations. Because of the thermal stresses induced by the cooling and the related reduction of effective normal stress, an increase in slip tendency of 0.2 can be calculated. However, modeled changes in the slip tendency are below those estimated to induce a possible reactivation of the faults and accompanied micro-seismic activities at the reservoir depth. This is in agreement with the observations done in the field (Kwiatek et al, 2010), where micro-seismic events have been recorded only during an extensive waterfrac stimulation treatment at the production well in 2007 (Zimmermann et al, 2010).

5 Discussion

Slip tendency analysis is a potential tool to identify critically stressed faults prone to reactivation. However, such an analysis is subjected to some uncertainty, as the magnitude of the in-situ stress state, in particular S_{Hmax}, is often not constrained, the friction coefficients of existing faults are usually not accurately known and the orientation of the stress tensor can vary spatially and stresses may rotate in the vicinity of faults (Jeanne et al, 2015). Furthermore, such an analysis does not take into account inelastic strain accumulation in the vicinity of fault zones. In aggregate this means that slip tendency analysis can only be used as an indication for the likelihood of fault reactivation and associated seismicity and not for predicting these events. In this study, the reactivation potential of existing faults was estimated relying on Terzaghi effective stress law. In the following we open a brief discussion touching upon these limiting aspects, mainly focusing on extending the current investigation to take into account the exact effective stress law (Nur and Byerlee, 1971) based on Biot theory of poro-elasticity and a failure criterion /other than Mohr-Coulomb) as based on true triaxial testing.

5.1 Failure criterion based on true triaxial testing

The present calculation of failure was based on the Mohr-Coulomb failure concept which is a 2D concept. Based on this failure criterion, induced seismicity associated to fast slip on a fault plane manifests as a result of the effective stress principle, where an increase in reservoir fluid pressure acts as reducing the effective normal stress acting on the fault plane, thus potentially leading the fault to fail.

The question remains if the waterfrac stimulation or the 30 years production and injection can lead to a failure of the intact rock sample in the vicinity of the reservoir operation. Moreover, the Mohr-Coulomb failure criterion neglects the additional role of the intermediate principal stress on fault reactivation, and the results as derived from this method should be always interpreted with caution. In this regard, other failure criteria for intact rock such that do consider the

intermediate principal stress in their formulation as the modified Lade 3D rock strength criterion (da Fontoura, 2012), three-dimensional failure criteria based on the Hoek-Brown criterion (Priest, 2012), or failure criteria for rocks based on true triaxial testing (Chang and Haimson, 2012) could be additionally considered. In what follows is a brief analysis of the simulation results based on the concept of a true triaxial failure mode. The experiments of Chang and Haimson (2012) demonstrated a systematic variation in rock strength as a function of σ_2. This approach is here applied to evaluate the stimulation treatment in Groß Schönebeck. The applied 3D failure criterion for brittle materials describes that failure occurs when the octahedral shear stress

$$\tau'_{oct} = \frac{1}{3}\sqrt{(\sigma'_1 - \sigma'_2)^2 + (\sigma'_2 - \sigma'_3)^2 + (\sigma'_3 - \sigma'_1)^2} \tag{12}$$

has reached a critical value in terms of the mean effective normal stress:

$$\sigma'_m = (\sigma'_1 + \sigma'_3)/2. \tag{13}$$

The failure envelopes obtained by laboratory experiments are power-law functions of the mean stress acting on the plane of failure:

$$\tau'_{oct} = A\sigma'^B_m \tag{14}$$

where A and B are material constants. The material constants reported for TCDP siltstone and KTB amphibolite are A = 2.32, B = 0.75 and A = 1.77, B = 0.86, respectively. For the clastic sediments at the geothermal test-site Groß Schönebeck, the values of the siltstone are most suitable. Therefore, failure will occur if

$$\frac{\tau'_{oct}}{2.32\sigma'^{0.75}_m} \geq 1. \tag{15}$$

The alteration of the in-situ stress state during stimulation and the corresponding tendency of failure is shown in Figure 6.

INSERT FIGURE 6 HERE

Both for **scenario one** and **scenario two**, the results indicate values of shear stresses which are higher in the vicinity of the stimulated area of the reservoir, with the former showing higher magnitudes than the latter. This last aspect is in agreement with the outcomes from the failure analysis based on the simplified Mohr-Coulomb criterion as discussed above which indicates the stress state as measured in the sandstone section of the reservoir to be more representative of the in-situ conditions (see also section 6). In both simulated scenarios, the failure envelope is not reached along the seismic plane, though **scenario one** indicates a propensity to failure at the base of the plane.

5.2 Biot exact effective stress law

In this subsection the results obtained by considering Biot's poro-elastic theory to investigate the potential of fault reactivation during the water frac treatment are

briefly discussed. By relying on Biot's theory, a stress coefficient $0 < \alpha < 1$ enters the effective stress concept (see Equation 1). In the case of Groß Schönebeck reservoir the effective stress coefficient α was approximated to be 0.6. When applying Biot's law, slip tendency values decreases by approximately 0.25 (**scenario one**) and 0.08 (**scenario two**) with respect to those obtained relying on Terzaghi's law (Figure 7). These low values in slip tendency require relatively (too) high overpressure (of similar magnitudes to those measured at the wellbore region) to be generated during stimulation activities (up to 39.3 MPa for **scenario one** and up to 64.7 MPa for **scenario two**) for fault reactivation to occur.

INSERT FIGURE 7 HERE

Though Biot's theory presents a more physically accurate description of the hydromechanical coupling in porous rocks, too few constraints on the static value of the Biot coefficient and, more importantly, of its dynamic evolution with loading conditions are available. This said, the results obtained in this paragraph should be considered as indicative lower bounds. Furthermore, the absolute principal stresses calculated based on field measurements were derived by relying on Terzaghi's law.

5.3 Reactivation of a pre-existing fault

The slip tendency analysis for **scenario one** indicates that failure conditions are reached at the bottom tip of the seismic plane during the waterfrac stimulation. For **scenario two**, which was calibrated with the stress state at the volcanic rock section, the slip tendency did not overcome the critical value of $\mu = 0.85$.

The measured seismic events during the 4th pressure cycle show an upward trend in their spatial distribution. The simulation result of **scenario one** indicates a higher potential at the bottom of the seismic plane, propagating upwards due to the waterfrac stimulation treatment. The combination of field observation and modelling results indicates that the seismic events occur along a pre-existing fault, directing approximately parallel to their best fitting plane. This pre-existing fault was not hydro-mechanical implemented in the presented simulation due to lack of information about geometry as well as mechanical and hydraulic properties. An implementation of this fault plane would lead to faster reservoir fluid pressure diffusion resulting in lower effective normal stresses and therefore to higher slip tendencies. In contrast, two neighboring faults show slip tendencies above a friction coefficient of $\mu = 0.85$ but no seismic events were recorded. This implies that the existence of these faults should be questioned. These observations ultimately could be supported by an ongoing interpretation of a 3D seismic campaign of the whole reservoir launched in 2017.

6 Conclusions

Based on a numerical model of coupled thermal-hydraulic-mechanical processes the fault reactivation potential and its alteration during a waterfrac stimulation treatment and a projected 30 years period of production and injection for the in-situ geothermal test-site Groß Schönebeck (Germany) was evaluated.

As pointed out in Section 2, two in-situ stress states were determined based on field measurements for the Groß Schönebeck geothermal reservoir, resulting in stress gradients for S_{hmin} up to 0.17 MPa/m. Such a stress gradient at this depth could not be explained by a variation of rock properties with depth and it was concluded that one of the provided stress states is most likely to be uncertain. The comparison of the measured micro-seismic events (location and temporal variability) with the model scenarios indicate that the stress state obtained for the sandstone section is more representative.

Considering this stress state the occurrence of the recorded micro-seismic events could be explained. In addition, the results indicate no potential for fault reactivation due to slip during 30 years of production and injection.

The presented numerical approach is a powerful tool to simulate the thermal, hydraulic, and mechanical processes in space and time. It can be adopted to evaluate the reservoir responses due to operation such as stimulation, production and injection. Therefore, it can be used to plan, evaluate and interpret reservoir operations and their potential risks.

References

Baisch S, Weidler R, Voros R, Wyborn D, de Graaf L (2006) Induced seismicity during the stimulation of a geothermal HFR reservoir in the Cooper Basin, Australia. Bulletin of the Seismological Society of America 96(6):2242–2256, DOI 10.1785/0120050255

Baisch S, Voros R, Weidler R, Wyborn D (2009) Investigation of fault mechanisms during geothermal reservoir stimulation experiments in the Cooper Basin, Australia. Bulletin of the Seismological Society of America 99(1):148–158, DOI 10.1785/0120080055

Baisch S, Voros R, Rothert E, Stang H, Jung R, Schellschmidt R (2010) A numerical model for fluid injection induced seismicity at Soultz-sous-Forêts. International Journal of Rock Mechanics and Mining Sciences 47(3):405–413, DOI 10.1016/j.ijrmms.2009.10.001

Bell JS (1996) In situ stresses in sedimentary rocks (Part 2): applications of stress measurements. Geoscience Canada 23:135–153

Blöcher G, Zimmermann G, Milsch H (2009) Impact of poroelastic response of sandstones on geothermal power production. Pure and Applied Geophysics 166(5-7):1107–1123, DOI 10.1007/s00024-009-0475-4

Blöcher G, Cacace M, Reinsch T, Watanabe N (2015) Evaluation of three exploitation concepts for a deep geothermal system in the North German Basin . Computers & Geosciences 82:120 – 129, DOI http://dx.doi.org/10.1016/j.cageo.2015.06.005

Blöcher G, Reinsch T, Henninges J, Milsch H, Regenspurg S, Kummerow J, Francke H, Kranz S, Saadat A, Zimmermann G, Huenges E (2016) Hydraulic history and current state of the deep geothermal reservoir Groß Schönebeck. Geothermics 63:27 – 43, DOI http://dx.doi.org/10.1016/j.geothermics.2015.07.008, enhanced Geothermal Systems: State of the Art

Blöcher MG, Zimmermann G, Moeck I, Brandt W, Hassanzadegan A, Magri F (2010) 3D numerical modeling of hydrothermal processes during the lifetime

of a deep geothermal reservoir. Geofluids 10(3):406–421, DOI 10.1111/j.1468-8123.2010.00284.x

Byerlee J (1978) Friction of rocks. Pure and Applied Geophysics PAGEOPH 116(4-5):615–626, DOI 10.1007/BF00876528

Cacace M, Jacquey AB (2017) Flexible parallel implicit modelling of coupled thermal–hydraulic–mechanical processes in fractured rocks. Solid Earth 8(5):921–941, DOI 10.5194/se-8-921-2017

Calò M, Dorbath C, Frogneux M (2014) Injection tests at the EGS reservoir of Soultz-sous-Forêts. Seismic response of the GPK4 stimulations. Geothermics 52:50–58, DOI 10.1016/j.geothermics.2013.10.007

Chang C, Haimson B (2012) A failure criterion for rocks based on true triaxial testing. Rock Mechanics and Rock Engineering 45(6):1007–1010, DOI 10.1007/s00603-012-0280-8

Deichmann N, Giardini D (2009) Earthquakes induced by the stimulation of an enhanced geothermal system below basel (Switzerland). Seismological Research Letters 80(5):784–798, DOI 10.1785/gssrl.80.5.784

Deichmann N, Kraft T, Evans KF (2014) Identification of faults activated during the stimulation of the basel geothermal project from cluster analysis and focal mechanisms of the larger magnitude events. Geothermics 52:84–97, DOI 10.1016/j.geothermics.2014.04.001

Dorbath L, Cuenot N, Genter A, Frogneux M (2009) Seismic response of the fractured and faulted granite of Soultz-sous-Forêts (France) to 5 km deep massive water injections. Geophysical Journal International 177(2):653–675, DOI 10.1111/j.1365-246X.2009.04030.x

Ellsworth WL (2013) Injection-induced earthquakes. Science 341(6142):1225,942–1225,942, DOI 10.1126/science.1225942

Engelder T (1993) Stress Regimes in the Lithosphere. Princeton University Press

Fehler M, Jupe A, Asanuma H (2001) More Than Cloud: New techniques for characterizing reservoir structure using induced seismicity. The Leading Edge 20(3):324–328, DOI 10.1190/1.1438942

da Fontoura SAB (2012) Lade and modified lade 3d rock strength criteria. Rock Mechanics and Rock Engineering 45(6):1001–1006, DOI 10.1007/s00603-012-0279-1

Fuchs K, Müller B (2001) World Stress Map of the Earth: a key to tectonic processes and technological applications. Naturwissenschaften 88:357–371

Gaston D, Newman C, Hansen G, Lebrun-Grandié D (2009) MOOSE: A parallel computational framework for coupled systems of nonlinear equations. Nuclear Engineering and Design 239(10):1768–1778, DOI 10.1016/j.nucengdes.2009.05.021

Gaucher E, Schoenball M, Heidbach O, Zang A, Fokker PA, van Wees JD, Kohl T (2015) Induced seismicity in geothermal reservoirs: A review of forecasting approaches. Renewable and Sustainable Energy Reviews 52:1473–1490, DOI 10.1016/j.rser.2015.08.026

Giardini D (2009) Geothermal quake risks must be faced. Nature 462:848–849, DOI 10.1038/462848a

Gupta H (2011) Encyclopedia of Solid Earth Geophysics. SPRINGER VERLAG GMBH

Hakimhashemi AH, Schoenball M, Heidbach O, Zang A, Grünthal G (2014a) Forward modelling of seismicity rate changes in georeservoirs with a hy-

brid geomechanical–statistical prototype model. Geothermics 52:185–194, DOI 10.1016/j.geothermics.2014.01.001

Hakimhashemi AH, Yoon JS, Heidbach O, Zang A, Grünthal G (2014b) Forward induced seismic hazard assessment: application to a synthetic seismicity catalogue from hydraulic stimulation modelling. Journal of Seismology 18(3):671–680, DOI 10.1007/s10950-014-9439-y

Häring MO, Schanz U, Ladner F, Dyer BC (2008) Characterisation of the Basel 1 enhanced geothermal system. Geothermics 37(5):469–495, DOI 10.1016/j.geothermics.2008.06.002

Healy JH, Rubey WW, Griggs DT, Raleigh CB (1968) The Denver EarthquakeS. Science 161(3848):1301–1310, DOI 10.1126/science.161.3848.1301

Jacquey AB, Cacace M, Blöcher G, Scheck-Wenderoth M (2015) Numerical investigation of thermoelastic effects on fault slip tendency during injection and production of geothermal fluids. Energy Procedia 76:311–320, DOI 10.1016/j.egypro.2015.07.868

Jacquey AB, Cacace M, Blöcher G, Watanabe N, Huenges E, Scheck-Wenderoth M (2016) Thermo-poroelastic numerical modelling for enhanced geothermal system performance: Case study of the Groß Schönebeck reservoir. Tectonophysics 684:119–130, DOI 10.1016/j.tecto.2015.12.020

Jaeger J, Cook NG, Zimmerman R (2007) Fundamentals of Rock Mechanics. Wiley-Blackwell

Jeanne P, Rutqvist J, Dobson PF, Garcia J, Walters M, Hartline C, Borgia A (2015) Geomechanical simulation of the stress tensor rotation caused by injection of cold water in a deep geothermal reservoir. Journal of Geophysical Research: Solid Earth 120(12):8422–8438, DOI 10.1002/2015jb012414

Jung R (2013) EGS – Goodbye or Back to the Future 95. In: Jeffrey R (ed) Effective and Sustainable Hydraulic Fracturing, InTech, chap 5, pp 95–121, DOI 10.5772/56458

Kwiatek G, Bohnhoff M, Dresen G, Schulze A, Schulte T, Zimmermann G, Huenges E (2010) Microseismicity induced during fluid-injection: A case study from the geothermal site at Groß Schönebeck and North German Basin. Acta Geophysica 58:995–1020, DOI 10.2478/s11600-010-0032-7

Kwiatek G, Bulut F, Bohnhoff M, Dresen G (2014) High-resolution analysis of seismicity induced at Berlín geothermal field, El Salvador. Geothermics 52:98–111, DOI 10.1016/j.geothermics.2013.09.008

Labuz JF, Zang A (2012) Mohr–Coulomb Failure Criterion. In: The ISRM Suggested Methods for Rock Characterization, Testing and Monitoring: 2007-2014, Springer International Publishing, pp 227–231, DOI 10.1007/978-3-319-07713-0-19

Lavrov A (2003) The Kaiser effect in rocks: principles and stress estimation techniques. International Journal of Rock Mechanics and Mining Sciences 40(2):151–171, DOI 10.1016/S1365-1609(02)00138-7

Mendecki A (2012) Seismic Monitoring in Mines. Springer Netherlands

Moeck I, Kwiatek G, Zimmermann G (2009) Slip tendency analysis, fault reactivation potential and induced seismicity in a deep geothermal reservoir. Journal of Structural Geology 31(10):1174–1182, DOI 10.1016/j.jsg.2009.06.012

Morris A, Ferrill DA, Henderson DB (1996) Slip-tendency analysis and fault reactivation. Geology 24(3):275, DOI 10.1130/0091-7613(1996)024¡0275:STAAFR¿2.3.CO;2

Nur A, Byerlee JD (1971) An exact effective stress law for elastic deformation of rock with fluids. Journal of Geophysical Research 76(26):6414–6419, DOI 10.1029/JB076i026p06414

Obermann A, Kraft T, Larose E, Wiemer S (2015) Potential of ambient seismic noise techniques to monitor the St. Gallen geothermal site (Switzerland). Journal of Geophysical Research: Solid Earth 120(6):4301–4316, DOI 10.1002/2014jb011817

Priest S (2012) Three-dimensional failure criteria based on the Hoek–Brown criterion. Rock Mechanics and Rock Engineering 45(6):989–993, DOI 10.1007/s00603-012-0277-3

Suckale J (2009) Induced seismicity in hydrocarbon fields. In: Advances in Geophysics, Elsevier, pp 55–106, DOI 10.1016/s0065-2687(09)05107-3

Talwani P, Acree S (1985) Pore pressure diffusion and the mechanism of reservoir-induced seismicity. Pure and Applied Geophysics PAGEOPH 122(6):947–965, DOI 10.1007/BF00876395

Trifu CIE (2010) Monitoring Induced Seismicity, vol Pageoph Topical Volumes. Birkhäuser, Basel

Zang A, Stephansson O (2010) Stress Field of the Earth's Crust. Springer

Zang A, Oye V, Jousset P, Deichmann N, Gritto R, McGarr A, Majer E, Bruhn D (2014) Analysis of induced seismicity in geothermal reservoirs – an overview. Geothermics 52:6–21, DOI 10.1016/j.geothermics.2014.06.005

Zimmermann G, Moeck I, Blöcher G (2010) Cyclic waterfrac stimulation to develop an Enhanced Geothermal System (EGS) - Conceptual design and experimental results. Geothermics 39(1):59–69, DOI 10.1016/j.geothermics.2009.10.003

Zoback MD (2007) Reservoir Geomechanics. Cambridge University Press (CUP), DOI 10.1017/CBO9780511586477

Zoback MD (2010) Reservoir Geomechanics, 2nd edn. Cambridge University Press (CUP), DOI 10.1017/CBO9780511586477

Zoback MD, Gorelick SM (2012) Earthquake triggering and large-scale geologic storage of carbon dioxide. Proceedings of the National Academy of Sciences 109(26):10,164–10,168, DOI 10.1073/pnas.1202473109

Table 1: In-situ stress state at the geothermal test-site Groß Schönebeck. S_V: vertical stress, S_{Hmax}: maximum horizontal stress, S_{hmin}: minimum horizontal stress and p_f reservoir fluid pressure (from Moeck et al, 2009). The stress state of the sandstone section and the volcanic rock section were used to calibrate model **scenario one** and **scenario two**, respectively.

Principal stresses	Sandstones section (4035 m TVDSS)	Volcanic rock section (4135 m TVDSS)
S_V (MPa)	100	103
S_{Hmax} (MPa)	98	105
S_{hmin} (MPa)	55	72
p_f (MPa)	43	43
Stress orientation S_{Hmax}	18.5° ± 3.7°	18.5° ± 3.7°
Stress regime	Normal faulting	Strike slip faulting

Table 2: Simulated in-situ stress state at the geothermal test-site Groß Schönebeck EGS. S_V: vertical stress, S_{Hmax}: maximum horizontal stress, S_{hmin}: minimum horizontal stress and p_f reservoir fluid pressure. The effective stresses were calculated by applying Terzaghi's effective stress law. The values were obtained in the sandstone section at 4035 m TVDSS and in the volcanic rock section at 4135 m TVDSS (UTM coordinates 33U 405250 mE 5862750 mN).

scenario one: calibrated in-situ stress state based on measurements in the sandstone section at 4035 TVDSS				
Principal stresses	Sandstones		Volcanic rocks	
	absolute (effective)	error [%]	absolute (effective)	error [%]
S_V (MPa)	100.2 (57.7)	0.2	102.7 (59.1)	0.3
S_{Hmax} (MPa)	98.2 (55.7)	0.2	101.4 (57.8)	3.4
S_{hmin} (MPa)	55.1 (12.6)	0.2	59.4 (15.8)	17.5
p_f (MPa)	42.6		43.6	
scenario two: calibrated in-situ stress state based on measurements in the volcanic rock section at 4135 TVDSS				
Principal stresses	Sandstones		Volcanic rocks	
	absolute (effective)	error [%]	absolute (effective)	error [%]
S_V (MPa)	100.1 (57.5)	0.1	102.5 (58.9)	0.5
S_{Hmax} (MPa)	101.8 (59.2)	3.9	104.9 (61.3)	0.1
S_{hmin} (MPa)	67.8 (25.3)	23.3	71.8 (28.2)	0.2
p_f (MPa)	42.6		43.6	

Table 3: Simulated reservoir fluid pressure p_f, temperature T, and slip tendency ST for the bottom tip of the micro-seismic events at -4221 m TVDSS. The values represents the in-situ state and the state at the end of the 4th pressure cycle of the performed waterfrac stimulation treatment (Figure 3 (bottom)).

Parameter	in-situ state	4th pressure cycle
scenario one		
p_f (MPa)	44.6	52.7
T (MPa)	150.5	150.5
ST (MPa)	0.71	0.92
scenario two		
p_f (MPa)	44.6	52.7
T (MPa)	150.5	150.5
ST (MPa)	0.41	0.42

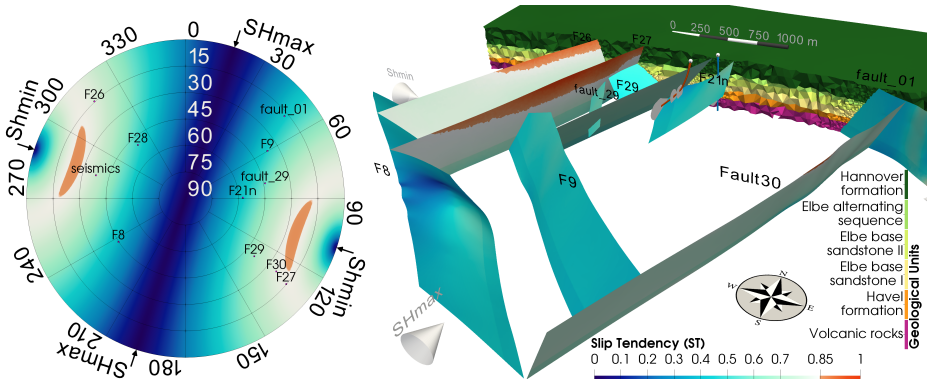

(a) (b)

Fig. 1: Slip tendency calculated by Terzaghi's effective stress law $\sigma'_n = \sigma_n - p_f$ calibrated for the in-situ stress state in the sandstone section at 4035 TVDSS (**scenario one**). Stereo plot of slip tendency including all considered fault planes (a) and distribution of slip tendency along the fault surfaces (b). Furthermore, the main geological units and the established geothermal doublet system consisting of a production well (deviated), injection well (vertical), and induced fractures (grey) are shown. (Color figure online)

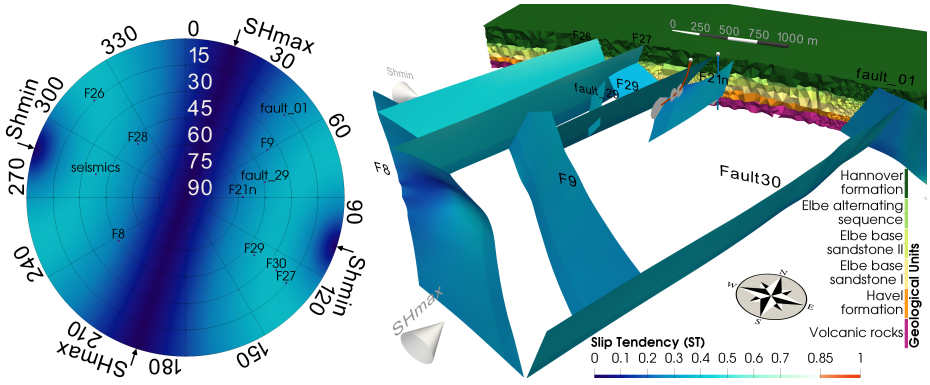

(a) (b)

Fig. 2: Slip tendency calculated by the Terzaghi's effective stress law $\sigma'_n = \sigma_n - p_f$ calibrated for the in-situ stress state in the volcanic rock section at 4135 TVDSS (**scenario two**). Stereo plot of slip tendency including all considered fault planes (a) and distribution of slip tendency along the fault surfaces (b). Furthermore, the main geological units and the established geothermal doublet system consisting of a production well (deviated), injection well (vertical), and induced fractures (grey) are shown. (Color figure online)

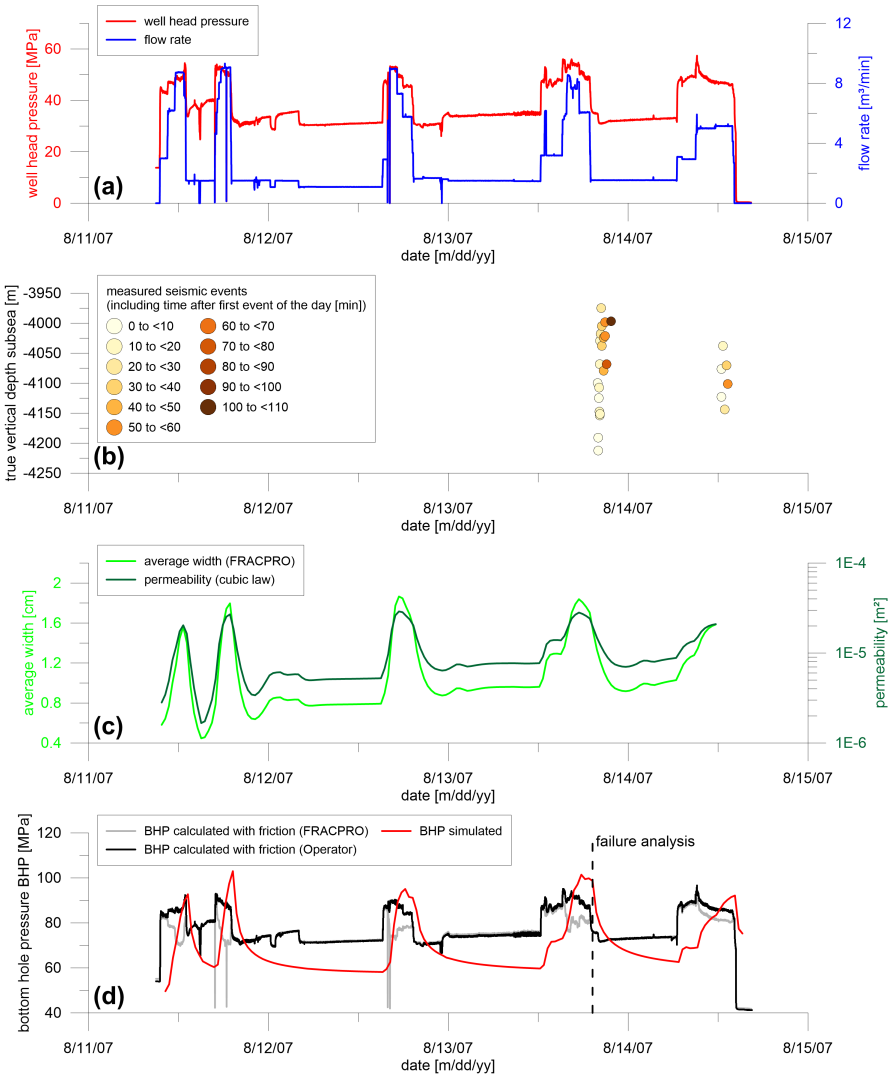

Fig. 3: Schedule of the waterfrac stimulation treatment carried out at the geothermal research well GtGrSk4/05 in Groß Schönebeck in 2007 (Zimmermann et al, 2010). Applied slurry rate at the well head and corresponding surface pressure (a); depth correlation of measured seismic events (Kwiatek et al, 2010) during the stimulation treatments (b); calculated average fracture width (FracPro) and corresponding fracture permeability (c); calculated and simulated bottom hole pressures (d). (Color figure online)

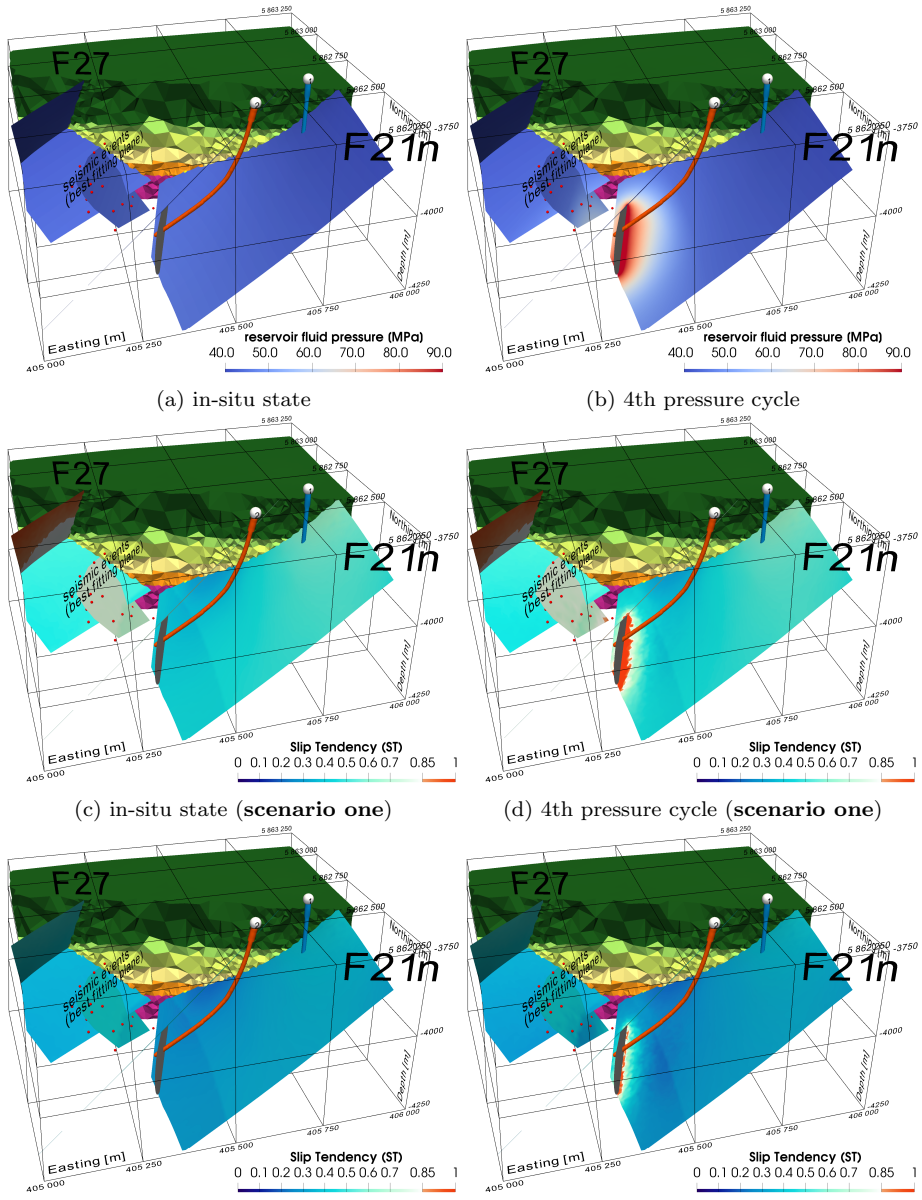

(a) in-situ state (b) 4th pressure cycle

(c) in-situ state (**scenario one**) (d) 4th pressure cycle (**scenario one**)

(e) in-situ state (**scenario two**) (f) 4th pressure cycle (**scenario two**)

Fig. 4: Simulated changes of reservoir fluid pressure (a,b) and slip tendency (c-f) due to waterfrac stimulation treatment carried out at the geothermal research well GtGrSk4/05 in Groß Schönebeck. (Color figure online)

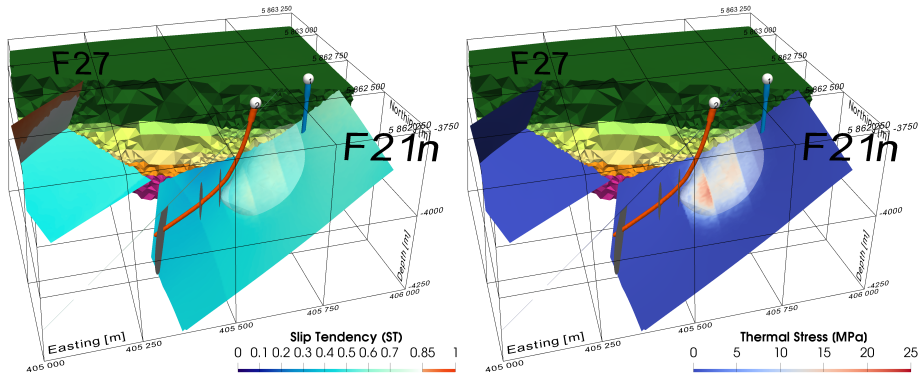

(a) (b)

Fig. 5: Simulated changes of slip tendency (a) and magnitude of thermal stresses (b) between the injection and production well due to 30 years of operation of the geothermal doublet system of Groß Schönebeck. The white bubble represents the 130° isotherm around the injection well. (Color figure online)

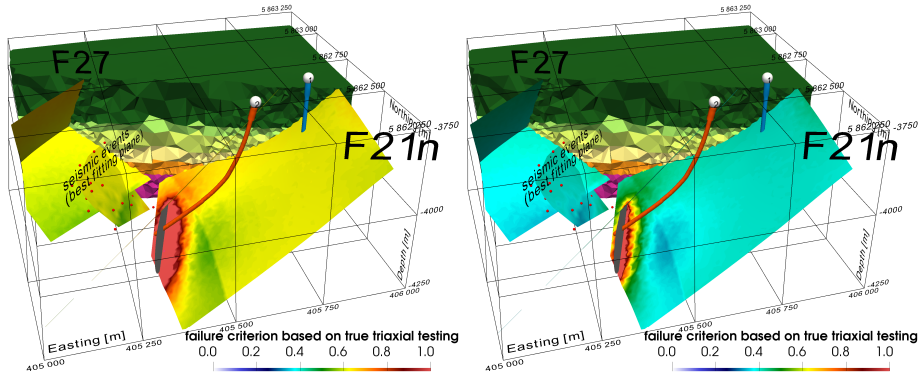

(a) **scenario one** (b) **scenario two**

Fig. 6: Changes of the in-situ stress state and the corresponding tendency of rock failure during the 4th pressure cycle of the waterfrac stimulation treatment at the geothermal test-site Groß Schönebeck using the three-dimensional failure criterion by Chang and Haimson (2012) (Color figure online)

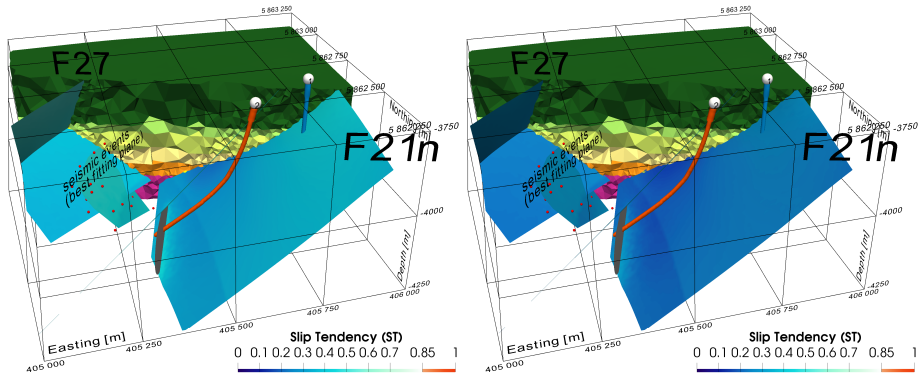

(a) **scenario one** (b) **scenario two**

Fig. 7: Simulated changes of slip tendency during the 4th pressure cycle of the waterfrac stimulation treatment at the geothermal test-site Groß Schönebeck. The results were obtained based on Biot's effective stress concept with an effective stress coefficient α of approximately 0.6. (Color figure online)